

THE COMPLEX MID-INFRARED STRUCTURE AT THE HEART OF IRAS 20126+4104

JAMES M. DE BUIZER

Gemini Observatory, La Serena, Chile; jdebuizer@gemini.edu

Received 2006 July 27; accepted 2006 November 29; published 2006 December 20

ABSTRACT

The mid-infrared emission at the center of IRAS 21026+4104 is not that of a simple compact source, as one would expect from an isolated high-mass protostellar object. Furthermore, the central thermal infrared emission does not appear to be coming directly from a circumstellar disk as has been recently hypothesized from near-infrared observations. The mid-infrared structure is complex, but with the help of multiple-wavelength information two plausible scenarios to explain the emission in the region are advanced. The first is that there is a tight cluster of young stellar objects here. The second is that the mid-infrared emission and masers are delineating the walls of the outflow cavities of a massive stellar source located in the center of the near- and mid-infrared dark lane.

Subject headings: circumstellar matter — infrared: ISM — ISM: individual (IRAS 20126+4104) — stars: early-type — stars: formation

1. INTRODUCTION

It is not clear whether massive stars in general form through accretion processes similar to low-mass stars. At present, the best example of a massive star with a possible accretion disk and bipolar outflow is considered to be IRAS 20126+4104 (see Cesaroni et al. 2007 for review). Originally thought to be a simple and compact high-mass protostellar object (aka hot molecular core), more recent observations by Cesaroni et al. (2005) have shown this source to be $\sim 7 M_{\odot}$, surrounded by a $R \sim 5000$ AU Keplerian rotating CS “disk,” with an outflow near perpendicular seen in H_2 and SiO. Whether this large “disk” is a circumstellar accretion disk or a accretion envelope feeding some unseen central accretion disk is still not understood.

Recent observations in the near-infrared (NIR) by Sridharan et al. (2005) revealed two K -band sources separated by a “dark lane,” interpreted as scattered emission on either side of a silhouette disk at the center of the larger rotating molecular “disk.” It was also concluded that the thermal emission from the $5 \mu\text{m}$ observations may be tracing the dust emission from the central accretion disk itself.

Observations at longer thermal infrared wavelengths are not hindered as much by extinction so are better tracers of the thermal dust emission that may be coming from the disk. In this article I describe recent high angular resolution mid-infrared (MIR) observations that reveal a much more complex dust structure than previously thought.

2. OBSERVATIONS

Observations were performed at Gemini North with the Michelle MIR imager and spectrograph. The instrument uses a Raytheon 320×240 pixel Si:As IBC array with a pixel scale of $0.099''$ pixel. $^{-1}$ Sky and telescope subtraction were achieved through the standard chop-nod technique. Imaging was performed using the Si-6 ($\lambda_c = 12.5 \mu\text{m}$, $\Delta\lambda = 1.2 \mu\text{m}$) filter and the Qa ($\lambda_c = 18.3 \mu\text{m}$, $\Delta\lambda = 1.6 \mu\text{m}$) filter. On-source exposure times of 282 and 82 s were used, respectively. Flux calibration was achieved by observing the MIR standard star HD 199101 at a an air mass similar to that of IRAS 20126+4104. Assumed flux densities for HD 199101 were taken to be 5.84 Jy at $12.5 \mu\text{m}$ and 2.63 Jy at $18.3 \mu\text{m}$. Flux densities measured are listed in Table 1. Uncertainties in these flux densities are estimated to be 10% at $12.5 \mu\text{m}$ and 15% at $18.3 \mu\text{m}$.

The images at both wavelengths were deconvolved using the maximum likelihood method (Richardson 1972; Lucy 1974). Since no natural point-spread function (PSF) stars were observed, artificially generated PSFs with FWHMs equal to the diffraction limit ($0.33''$ at $12.5 \mu\text{m}$ and $0.48''$ at $18.3 \mu\text{m}$) were used in the deconvolutions. The deconvolution routine was stopped at 25 iterations for the $12.5 \mu\text{m}$ image and 50 iterations for the $18.3 \mu\text{m}$ image. These deconvolved images compare favorably to simple unsharp masking of the original images, and thus the revealed substructures in the deconvolved images are believed to be real.

The relative astrometry between the NIR (K , L , and M) and the MIR images was accurately determined due to the presence of two (M) or three (K and L) common point sources in the field. The mean residual offset between the $12.5 \mu\text{m}$ and NIR images was found to be less than a Michelle pixel ($0.099''$) in all cases ($0.04''$ for K , $0.03''$ for L , and $0.09''$ for M).

3. RESULTS

Figure 1 shows a portion of the deconvolved $12.5 \mu\text{m}$ field centered on the coordinates of the 1.3 cm radio continuum peak of P. Hofner et al. (2007, in preparation). Near the origin is a bright MIR double source (IRAS 20126+4104:D06 1 and IRAS 20126+4104:D06 2, from now on these will be referred to as simply D06 1 and D06 2). These MIR sources, like the double source seen at K by Sridharan et al. (2005), have a “dark lane” separating them. Most importantly, the dark lane between the K -band sources, which is hypothesized by Sridharan et al. (2005) to be the “absorption lane” of the NIR silhouette disk, is exactly coincident with the dark lane between the two mid-infrared sources.

Figure 2 shows that the comparisons between the MIR images and the L and M images of Sridharan et al. (2005). The M peak is coincident with the MIR emission from D06 2. Consequently, this means that the M peak is not located in the dark lane as suggested by Sridharan et al. (2005). Since this NIR dark lane is also the location of minimum flux density between the MIR sources D06 1 and D06 2, and D06 2 is coincident with the M peak, the suggestion by Sridharan et al. (2005) that the longer wavelength NIR emission is tracing thermal dust emission from a near edge-on circumstellar disk inside the dark lane between the K -band sources is not confirmed.

The secondary peak seen at L by Sridharan et al. (2005) is

TABLE 1
OBSERVED AND DERIVED PARAMETERS

| Source | $F_{12.5\ \mu\text{m}}$ (Jy) | $F_{18.3\ \mu\text{m}}$ (Jy) | $L_{\text{MIR}}^{\text{a}}$ (L_{\odot}) | Spectral Type ^a |
|----------------------------------|---------------------------------|---------------------------------|--|----------------------------|
| D06 1 | 0.71 | 3.71 | 58 | B9 |
| D06 2 | 0.34 | 2.97 | 63 | B9 |
| Double source ^b | 1.06 | 6.45 | 106 | B8 |
| Whole field ^c | 1.89 | 23.5 | 715 | B5 |

NOTE.—Accuracy of the flux densities: 10% at 12.5 μm , 15% at 18.3 μm .

^a These are lower limits to the luminosity and spectral type derived from the MIR flux densities and assuming that all emission is from a single stellar source. See De Buizer et al. (2005) for techniques and assumptions.

^b Flux density in a 1.0'' radius aperture around D06 1 and D06 2 only.

^c Flux density in a 8.0'' radius aperture encompassing all MIR sources.

found to be coincident with a MIR extension to the south of the MIR double source in the deconvolved 12.5 μm image (labeled the “southern extension” in Fig. 1). Another MIR extension to the west of the D06 1 is weak at 12.5 μm , but is clearly evident and resolved from the double source at 18.3 μm (labeled the “western extension” in Fig. 1). One further difference between the 12.5 and 18.3 μm deconvolved images is the shape of D06 1. At 18.3 μm

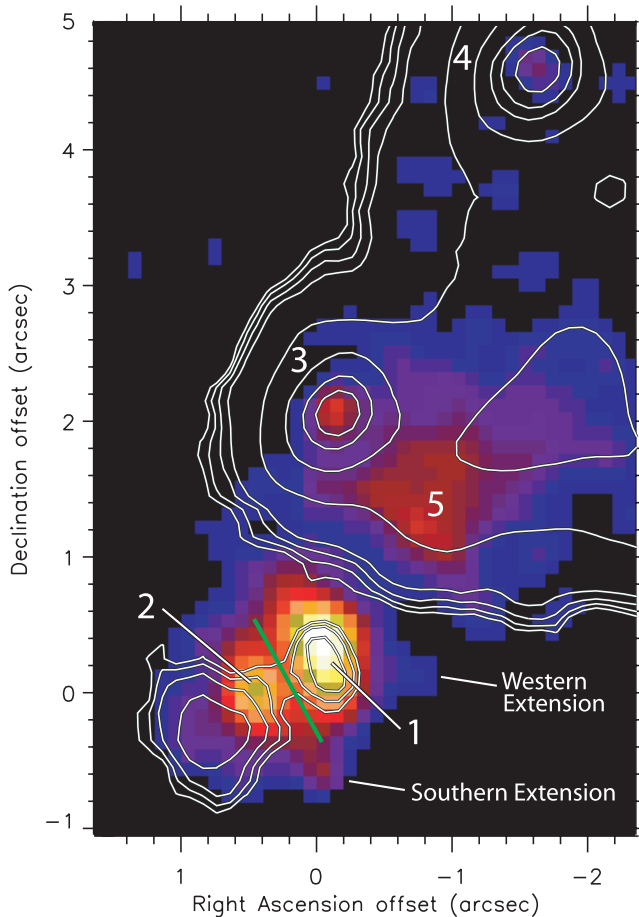


FIG. 1.—The 12.5 μm deconvolved Michelle image of IRAS 20126+4104 in false color overlaid with the K -band contours of Sridharan et al. (2005). Three common sources (only two sources, D06 3 and 4, are shown here) in the field were used to accurately register the MIR and NIR images. The green line shows the location of the NIR/MIR dark lane. The origin of the figure is the location of the P. Hofner et al. (2007, in preparation) 1.3 cm radio continuum peak (R.A. = 20^h14^m26.031^s, decl. = 41^o13'32.58" [J2000.0]).

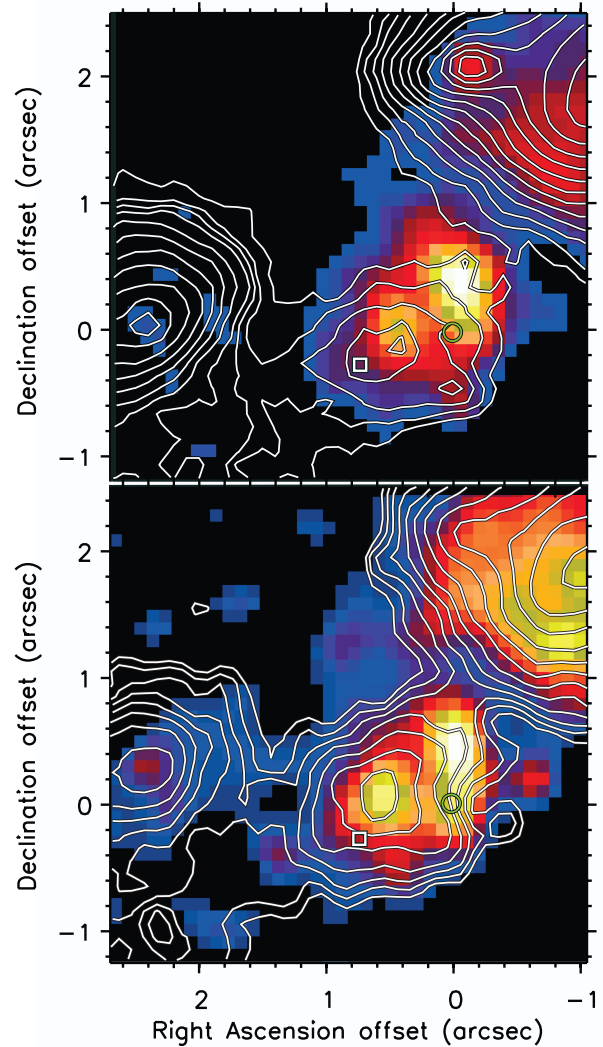


FIG. 2.—Comparisons between MIR and NIR morphologies. The top panel shows the deconvolved 12.5 μm image in false color overlaid with the L -band contours of Sridharan et al. (2005). The bottom panel shows the deconvolved 18.3 μm image in false color overlaid with the M -band contours of Sridharan et al. (2005). The origins are the same as Fig. 1. The locations of the 1.3 cm radio continuum peak (green circle) and the southeastern K -band peak (white square) are shown.

the source is elongated further to the south ($\sim 0.2''$) than at 12.5 μm (see Fig. 2).

Figure 3 shows the comparison of the 18.3 μm deconvolved image to several other wavelengths known to have very good ($\leq 0.15''$) absolute astrometric accuracy. The K -band image (blue contours) of Sridharan et al. (2005) is claimed to be known to an absolute astrometric accuracy of 0.15''. Because the relative registration between the NIR and MIR images is shown to be better than 0.1'', the absolute position error of the MIR image is therefore the quadrature addition of these two values, namely, $< 0.18''$.

Also shown in Figure 3 are the locations of OH, water, and methanol masers from Edris et al. (2005). The absolute astrometry of these masers are known to better than 25 mas. Also plotted in Figure 3 are the three water maser locations of Tofani et al. (1995), which appear to be associated with the locations of D06 1 and 2 and the MIR western extension. The 3.6 cm radio continuum

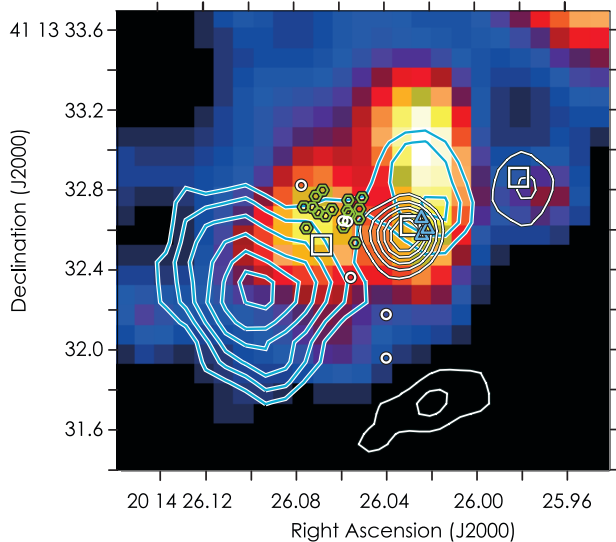


FIG. 3.—Deconvolved $18.3 \mu\text{m}$ image in false color is overlaid with contours from several wavelengths. The blue contours are the K -band contours of Sridharan et al. (2005), the white contours are the 3.6 cm radio continuum emission from P. Hofner et al. (2007, in preparation). The water masers (white squares) of Tofani et al. (1995) are shown, as well as the OH (white circles), water (blue triangles), and methanol masers (green pentagons) from Edris et al. (2005).

(white contours) from P. Hofner et al. (2007, in preparation) are also shown in Figure 3. The brightest radio component has a peak near the southern elongation of D06 1 seen at $18.3 \mu\text{m}$. The westernmost radio continuum component lies very close ($<0.1''$) to the MIR western extension. The radio continuum component to the south has no associated MIR emission.

Figure 3 shows a complex distribution of multiwavelength emission; however, the astrometric precision of all of these observations facilitates the interpretation of the combined data set. Two possible scenarios will now be forwarded that may explain the observed complexity, although further data will be required to test either scenario. The first scenario is that there is a cluster of young sources present at the center of IRAS 210126+4104, and the second is that the different wavelengths of emission are coming from different tracers of the bipolar outflow from this region centered on the dark lane seen in the NIR and MIR.

3.1. Multiple Source Scenario

The heart of IRAS 210126+4104 may contain a small cluster of young stellar sources of various masses and in various stages of formation. There could be several individual sources here, among them could be D06 1, D06 2, each of the three radio continuum peaks. These sources would have various associations, for instance, D06 2, which is coincident with the peak seen by Sridharan et al. (2005) at M , as seen in Figure 2. This source is also traced by copious amounts of methanol, OH, and water maser emission, but has no radio continuum emission of its own. Based solely on the MIR luminosity and assuming emission from a single stellar source, a lower limit to the spectral type for D06 2 of B9 was derived (Table 1) using the methods of De Buizer et al. (2005). In contrast, the source associated with the brightest radio continuum peak does not appear to have any directly related MIR emission at $12.5 \mu\text{m}$, and based on the work of Hofner et al. (1999) could be an embedded ultracompact H II region of a star of spectral type B3. However, the MIR

emission of D06 1 does extend toward this source at $18.3 \mu\text{m}$ and may be marking the weak emission at longer MIR wavelengths from the radio continuum source. In this multiple source scenario, the dark lane seen in the NIR and MIR would simply be a space separating the various IR sources present, like the “dark lane” between D06 1 and D06 5.

This scenario of having more than one young stellar source at the heart of IRAS 20126+4104 could help to explain the detection of apparently two outflows from this region: one nearly north-south and the other northwest-southeast, and with redshifted and blueshifted lobes reversed in the two cases (Cesaroni et al. 2005). These outflows could come from two independent stellar sources, as has been suggested before (e.g., Lebrón et al. 2006). Given its central location with respect to the overall NIR/MIR emission as well as the H_2 outflow, and its association with the majority of the masers in the region, D06 2 could be the dominant young stellar object in the cluster in this scenario.

Hofner et al. (1999) point out that if the three radio peaks are considered to be three zero-age main-sequence stars of spectral type B3 (as indicated by their radio continuum emission), there is a problem accounting for the total luminosity of the region at far-infrared (FIR) wavelengths. Three such stars combined would have a luminosity of only $3.0 \times 10^3 L_\odot$, but the FIR luminosity measured by IRAS is $1.3 \times 10^4 L_\odot$. But if just one of these MIR sources without radio continuum emission (i.e., D06 2) is a high-mass protostellar object (HMPO), then this could explain the higher flux densities at FIR wavelengths since it is at these longer wavelengths that the spectral energy distributions of HMPOs peak.

3.2. IR Emission from Outflow Scenario

Sridharan et al. (2005) assert that the dark lane between the K -band sources is an “absorption lane” of a silhouette disk of a young massive stellar source and that the longer wavelength IR emission comes from the dust emission of the accretion disk in this absorption lane. However, the NIR and MIR emission share a common dark lane between the northwestern and southeastern sources of IR emission. In this section an alternate scenario is proposed in which this dark lane is indeed an absorption lane of an embedded stellar source; however, it is instead argued that both the NIR and MIR are coming from scattered and direct emission, respectively, off the outflow cavities from this stellar source.

Figure 3 shows that all of the maser species are predominantly situated along the inner edges of the absorption lane but are associated with the infrared emission and not the lane itself (contrary to what is claimed by Edris et al. [2005] on the basis of NIR data alone). Therefore, a more simplistic scenario could be that the masers and MIR emission are delineating the walls of the cavities of an outflow coming from the massive embedded star at the center of the absorption lane. The NIR, MIR, radio continuum, and maser emission in this region would be coming from different parts of the northwest and southeast outflow cavities. The outflow axis seen in H_2 , SiO , and HCO^+ (Cesaroni et al. 1999) has a position angle close to $\theta \sim -60^\circ$. The dark lane seen in the MIR lies at $\theta \sim 30^\circ$ (Fig. 1), perpendicular to the outflow. The other extended MIR emission components in the field (IRAS 21026+4104:D06 5, and perhaps D06 3 and D06 4 in Fig. 1) lie close to this outflow axis and may be outflow-related MIR emission since they are coincident with K and H_2 emission here.

The two northern knots of radio continuum emission in Fig-

ure 3 are hypothesized by P. Hofner et al. (2007, in preparation) to perhaps be a part of a outflow jet emanating from a stellar source located in the IR dark lane. This jet is aligned slightly more east-west ($\theta \sim -70^\circ$) than the outflow seen in H_2 , SiO , and HCO^+ , and is much different than the larger scale CO outflow (Lebrón et al. 2006) that appears closer to north-south ($\theta \sim -25^\circ$). The high shock temperature required to excite the H_2 $v = 1-0$ $S(1)$ transition is several thousand degrees, whereas for CO ($J = 2-1$) it is just a few kelvins. H_2 rapidly cools below the temperature where it can emit in a timescale of ~ 1 yr (Le Bourlot et al. 1999). However, the CO remains excited in the postshock gas (since the gas temperature here is in excess of the ~ 5 K needed for this to happen), thus providing a fossil record of the outflow shock interaction. Therefore instead of being due to multiple outflowing sources as described in the last section, there may be one wandering outflow responsible for the apparent array of outflow angles seen. The CO could be indicating the past history of the outflow, whereas the H_2 and radio continuum emission is denoting what is occurring more recently.

In this outflow cavity scenario, the southeastern component of the double source at K and the MIR emission from D06 2 would be tracing different parts of the southeastern outflow cavity. Cesaroni et al. (2005) finds that the high-velocity outflowing gas is redshifted to the southeast and blueshifted to the northwest. Therefore the disk is not exactly edge-on, and we expect to have a more direct and unextinguished view of the northwestern outflow cavity than the southeastern. The southeastern NIR and MIR emission is extended on the same scale; however, the MIR peak is closer to the absorption lane than the NIR peaks. The emission in the MIR of D06 2 may be seen closer to the dark lane because the MIR emission penetrates more easily through obscured areas and is generally orders of magnitude less efficiently scattered than K emission in an outflow cavity. This holds true under the general assumption that there is not a large variation in the dust composition and size distribution throughout this whole region. Assuming this to be true, the emission in the thermal IR (MIR and M) in the southeastern cavity would appear closest to the absorption lane, at L the peak is further out, and at K even further out.

Given the more favorable viewing angle and with extinction playing less of a role, we have a more direct view of the northwestern outflow cavity. This means we can directly see the hot dust down closer to the stellar source itself at L and M . This, plus resolution effects due to the fact that the emission from above and below the dark lane are closer together at L and M than at K , may account for the fact that the extinction lane is not as prominent at these wavelengths. The K emission may be seen further out due to the efficiency with which it scatters, and MIR emission may be further out because it is tracing the cooler dust. This, combined with the better reso-

lution at these wavelengths may help to enhance the appearance of the dark lane at K and in the MIR.

The MIR southern extension may also be better explained by the outflow cavity scenario. The emission at this location is not apparent at K , bright at L , marginally detected at M , present at $12.5 \mu\text{m}$, and shifted in location at $18.3 \mu\text{m}$. If the emission is coming from an outflow region, it is plausible that line emission, temperature and optical depth gradients, and scattering could cause the infrared emission peaks to move as a function of wavelength within the outflow cavity. However, further data, including spectroscopy, will be required to know the true nature of the southern extension. The main point, however, is that this behavior as a function of wavelength could not be due to a stellar “binary companion,” as suggested by Sridharan et al. (2005), as dusty young stellar sources have increasing flux density as a function of increasing wavelength.

The outflow scenario also fits well the observed maser properties. Moscadelli et al. (2000, 2005) have already shown that their observations of the water maser spots can be well fit to a model where they are moving outward from the location of the dark lane along the axis of outflow. In a similar fashion, here it is suggested that the methanol maser emission is associated with the inner parts of the southeastern outflow cavity. This matches recent observations indicating that methanol masers are associated with the outflows from young massive stars (e.g., De Buizer 2003, 2006).

Assuming that the unseen stellar source at the center of the dark lane is responsible for radio continuum emission in outflow, Hofner et al. (1999) derived a B1 spectral type for this central star under the assumption that the radio continuum emission is beamed emission into the jet cavity. All of the extended MIR emission could indeed be heated by a single B1 star as well. The farthest MIR source, D06 4, is ~ 8500 AU away from the radio continuum peak, but assuming smooth astronomical silicates and small grains, it is possible to heat dust to ~ 120 K out to this distance (see De Buizer 2006). Therefore, all of the MIR emission observed to be associated with IRAS 21026+4104 requires no more than a single B1 stellar source at its heart, and a multiple source scenario is not necessary. However, it is possible that there are other young stellar sources (perhaps D06 3, 4, and 5) present and helping to heat the dust in the regions farther from the center.

Many thanks to T. K. Sridharan and P. Hofner for their valuable help. This work is based on observations obtained at the Gemini Observatory, which is operated by the AURA, Inc., under a cooperative agreement with the NSF on behalf of the Gemini partnership: NSF (US), PPARC (UK), NRC (Canada), CONICYT (Chile), ARC (Australia), CNPq (Brazil), and CONICET (Argentina). The Gemini program identification number associated with the data is GN-2005B-Q-21.

REFERENCES

- Cesaroni, R., Felli, M., Jenness, T., Neri, R., Olmi, L., Robberto, M., Testi, L., & Walmsley, C. M. 1999, *A&A*, 345, 949
 Cesaroni, R., Galli, D., Lodato, G., Walmsley, C. M., & Zhang, Q. 2007, in *Protostars and Planets V*, ed. V. Mannings et al. (Houston: LPI), in press
 Cesaroni, R., Neri, R., Olmi, L., Testi, L., Walmsley, C. M., & Hofner, P. 2005, *A&A*, 434, 1039
 De Buizer, J. M. 2003, *MNRAS*, 341, 277
 ———. 2006, *ApJ*, 642, L57
 De Buizer, J. M., Radomski, J. T., Telesco, C. M., & Piña, R. K. 2005, *ApJS*, 156, 179
 Edris, K. A., Fuller, G. A., Cohen, R. J., & Etoke, S. 2005, *A&A*, 434, 213
 Hofner, P., Cesaroni, R., Rodríguez, L. F., & Martí, J. 1999, *A&A*, 345, L43
 Le Bourlot, J., Pineau des Forêts, G., & Flower, D. R. 1999, *MNRAS*, 305, 802
 Lebrón, M., Beuther, H., Schilke, P., & Stanke, T. 2006, *A&A*, 448, 1037
 Lucy, L. B. 1974, *AJ*, 79, 745
 Moscadelli, L., Cesaroni, R., & Rioja, M. J. 2000, *A&A*, 360, 663
 ———. 2005, *A&A*, 438, 889
 Richardson, W. H. 1972, *J. Opt. Soc. Am.*, 62, 55
 Sridharan, T. K., Williams, S. J., & Fuller, G. A. 2005, *ApJ*, 631, L73
 Tofani, G., Felli, M., Taylor, G. B., & Hunter, T. R. 1995, *A&AS*, 112, 299